Published OnlineFirst April 16, 2014; DOI: 10.1158/1535-7163.MCT-13-0962

Molecular Cancer Therapeutics

Targeting Integrin α6 Stimulates Curative-Type Bone Metastasis Lesions in a Xenograft Model

Terry H. Landowski[1,2], Jaime Gard[1], Erika Pond[1], Gerald D. Pond[3], Raymond B. Nagle[1,4], Christopher P. Geffre[4], and Anne E. Cress[1,5]

Abstract

Laminin-binding integrin receptors are key mediators of epithelial cell migration and tumor metastasis. Recent studies have demonstrated a role for the α6 integrin (ITGA6/CD49f) in maintaining stem cell compartments within normal bone marrow and in residency of tumors metastatic to bone. In this study, we tested a function-blocking antibody specific for ITGA6, called J8H, to determine if preexisting cancer lesions in bone could be slowed and/or animal survival improved. Human prostate tumors were established by intracardiac injection into male SCID mice and treatment with J8H antibody was initiated after 1 week. Tumor progression was monitored by micro-computed tomography (CT) imaging of skeletal lesions. Animals that received weekly injections of the anti-ITGA6 antibody showed radiographic progression in only 40% of osseous tumors (femur or tibia), compared with control animals, where 80% of the lesions (femur or tibia) showed progression at 5 weeks. Kaplan–Meier survival analysis demonstrated a significant survival advantage for J8H-treated animals. Unexpectedly, CT image analysis revealed an increased proportion of bone lesions displaying a sclerotic rim of new bone formation, encapsulating the arrested lytic lesions in animals that received the anti-ITGA6 antibody treatment. Histopathology of the sclerotic lesions demonstrated well-circumscribed tumor within bone, surrounded by fibrosis. These data suggest that systemic targeting of the ITGA6-dependent function of established tumors in bone may offer a noncytotoxic approach to arrest the osteolytic progression of metastatic prostate cancer, thereby providing a new therapeutic strategy for advanced disease. *Mol Cancer Ther; 13(6); 1558–66. ©2014 AACR.*

Introduction

Prostate cancer is the most frequently diagnosed noncutaneous malignancy in North America and is the second leading cause of cancer deaths in men. The most debilitating and life-threatening aspect of advanced prostate cancer is the propensity of the tumor to metastasize to bone. Approximately 85% of patients with advanced disease have bone metastases (1, 2). Recent genomic analyses of primary versus metastatic tumor has suggested that in highly metastatic tumors, such as prostate, breast, and lung carcinomas, micrometastases in the bone marrow may occur very early in the natural history of the disease. This early dissemination of malignant cells has been proposed as the basis for widespread recurrence, which can occur as aggressive skeletal metastatic disease up to 10 years after primary therapy (3, 4). Prostate cancer is fundamentally an indolent tumor and preventing the progression of early bone metastases may have a significant impact on survival and quality of life (5, 6).

The α6 integrin (ITGA6/CD49f), a laminin receptor, is expressed on human prostate tumors and is associated with poor patient prognosis, reduced survival, and increased metastasis in a variety of tumors (7–10). ITGA6 is also expressed by human hematopoietic stem cell populations and is coincident with abundant laminin 511 in normal human bone (11–13). The ITGA6 ligand, laminin 511 (LN511), is an essential component of the stem cell niche and supports stem cell survival independent of additional cytokines or growth factors (14, 15). These observations suggest that the ITGA6–LN511 interaction is a fundamental feature of both stem cells and tumors within the bone marrow microenvironment and that this interaction may provide a therapeutic opportunity for systemic treatment of metastatic tumors.

A tumor-specific form of ITGA6, called α6p, is generated by coordinated proteolytic removal of the laminin-binding domain from the tumor cell surface by urokinase-type plasminogen activator (uPA), a prometastatic factor (16, 17). Expression levels of both uPA and its cognate receptor are negatively correlated with prostate cancer patient survival (18, 19). Our previous work has demonstrated that inhibition of ITGA6 cleavage function

Authors' Affiliations: [1]University of Arizona Cancer Center; Departments of [2]Medicine, [3]Medical Imaging, [4]Pathology, and [5]Cellular and Molecular Medicine, University of Arizona Cancer Center, Tucson, Arizona

Corresponding Author: Anne E. Cress, University of Arizona Cancer Center, 1515 N. Campbell Avenue, Tucson, AZ 85724. Phone: 520-626-7553; Fax: 520-626-4568; E-mail: cress@email.arizona.edu

doi: 10.1158/1535-7163.MCT-13-0962

Published OnlineFirst April 16, 2014; DOI: 10.1158/1535-7163.MCT-13-0962

will significantly inhibit tumor migration both *in vitro* and *in vivo* (20, 21). To further understand the molecular requirements for ITGA6 in bone marrow metastases, we have established a xenograft model of treatment for early tumor dissemination. After tumor cell seeding within bone from the circulation, an anti-ITGA6 function blocking monoclonal antibody (J8H) was administered weekly and the progression of bone lesions monitored weekly by micro-CT analysis, followed by image matched histopathology. Inhibition of ITGA6 cleavage blocked tumor progression and increased overall survival. Animals treated with the J8H antibody displayed a higher frequency of lesions with morphologic characteristics of a sclerotic response. These data suggest that agents that target ITGA6 and modulate the migration phenotype may provide a noncytotoxic alternative for patients with metastatic bone disease.

Materials and Methods

Cells

The PC3B1a cells are a bone-homing subclone of the PC3 human prostate cancer cell line previously described (21, 22). Cells were maintained in Iscove's modified Dulbecco's medium (IMDM; Life Technologies) supplemented with 10% heat-inactivated FBS (Hyclone Laboratories) at 37°C in a 5% CO_2 atmosphere at constant humidity. Cell line identity was validated within 6 months using short tandem repeat (STR) analysis by the Human Origins Genotyping Laboratory (HOGL) at the University of Arizona.

Antibodies

The mouse monoclonal antibody, J8H, created by Dr. A. Sonnenberg (23), recognizes an extracellular epitope of ITGA6. For *in vivo* administration, endotoxin-free J8H antibody was produced and purified by BIOCULT (Roelofarendsveen, the Netherlands) and resuspended in sterile saline for intravenous administration. For *in vitro* characterizations, rat monoclonal antibody J1B5 (generated by Dr. C.H. Damsky; ref. 24), and GoH3 (generated by Dr. A. Sonnenberg; ref. 25), both of which recognize an extracellular epitope of ITGA6, were used. A6NT, a rabbit polyclonal antibody, was generated against a recombinant fragment of the NH_2-terminal ITGA6 β-barrel domain (21). The AIIB2 function blocking antibody for the β1 integrin (ITGB1/CD 29) was obtained from the Developmental Studies Hybridoma Bank, University of Iowa.

Cell adhesion assay

Each well of a 96-multiwell plate was coated with laminin 511. Laminin was isolated from the conditioned media (CM) of A549 cells as previously described (26). The wells were blocked with 100 μL of 1% BSA for 1 hour. PC3B1a cells (5×10^4) were suspended in serum-free IMDM with or without 1 mg/mL of the indicated antibody and incubated for 60 minutes at 37°C. Wells were washed 3 times with PBS and fixed with 2.5% formaldehyde. The adherent cells were stained with 0.5% crystal violet in 20% (v/v) methanol/water, the dye solubilized using 0.1M sodium citrate, and absorbance at 562 nm wavelength was determined. Data shown are the mean of triplicate determinations.

Cell migration assay

Cell culture inserts (BD Biosciences) with 8 μm pores were coated overnight at 4°C on the underside of the insert with 50 μL of conditioned media containing laminin 511 (26). The coated inserts were placed into wells containing 600 μL IMDM plus 10% FBS in a 24-well tissue culture plate. Approximately 15,000 cells in 200 μL of serum-free IMDM were incubated with or without inhibitor for 1 hour at 37°C, before plating in the upper chamber of each insert and additional incubation for 5 hours at 37°C. The inserts were washed in PBS and cells on the underside of the insert were fixed and permeabilized in methanol/acetone and stained with 4′,6-diamidino-2-phenylindole (DAPI; 1 μg/mL; Sigma Chemical Co.) for nuclei detection. The cell numbers were counted using a Zeiss Axiophot inverted fluorescent microscope at ×200 magnification. The cells were counted in 5 sections of each insert (4 corners and the middle) to obtain the total number of cells migrating per insert. Experiments were performed twice in triplicate, and the average number of cells per insert was calculated.

SCID mouse xenograft model

Animal experiments were conducted with animal care and use committee approval using the facilities and staff of the Experimental Mouse Shared Service at The University of Arizona Cancer Center. Left ventricle injections of single-cell suspensions of ~0.5 million cells in 0.2 mL PBS were done with a 27-gauge needle as described previously (21, 27). Mice were anesthetized with isoflurane (2%–3%, delivered through a nose cone). Twelve mice were used in each treatment group as dictated by statistical power analysis. One-way ANOVA between 2 treatment groups was used as the model with an 80% chance of detecting a difference and no more than a 5% chance of error. Mice receiving incorrectly placed injections indicated by chest tumors at necropsy were removed from the study. Animals were terminated by CO_2 inhalation if microfractures were detected by micro-CT, if they showed signs of pain/suffering, or in the case of unexplained weight loss as specified by protocol. Survival advantage was determined using log-rank analysis of the Kaplan–Meier survival time.

Micro-CT analysis

Micro-CT scans were performed before tumor injection, and each week from 3 to 7 weeks after tumor cell injection using a Siemens Inveon micro-CT Scanner. Required calibrations (i.e., center-offset calibration and light/dark calibration) for the selected CT scan protocol were done before scanning test animals. Animals were anesthetized with 4% isoflurane in an anesthesia chamber. After the scan, 1 mL of sterile saline was injected subcutaneously to

Published OnlineFirst April 16, 2014; DOI: 10.1158/1535-7163.MCT-13-0962

aid recovery. Micro-CT image interpretation and analysis was done using Inveon Research Workplace (IRW) software. CT scans were reviewed and scored weekly by a radiologist (G.D. Pond) without knowledge of the treatment groups. Subjects were identified as having progressive lesions if the lesions increased in size in all 3 views (axial, coronal, and sagittal). The specific anatomical location of the identified lesions was recorded and lesions were individually followed for up to 8 weeks.

Senescence assay

PC3B1a cells were incubated in serum-deprived media (0.5% FBS in IMDM), with or without J8H antibody, for 24 to 72 hours to generate PC3B1a CM. The conditioned media from J8H immobilized or control PC3B1a cells was collected at the indicated time point and analyzed using the human cysteine-rich protein 61 (Cyr61/CCN1) DuoSet ELISA from R&D Systems. Function analysis of the PC3B1a CM was done using a Quantitative Fluorescence Senescence Assay Kit (Cell Biolabs, Inc.). Human foreskin fibroblast (HFF) cells were incubated for 72 hours in serum-deprived media (0.5% FBS in IMDM) with or without recombinant human Cyr61 at 5 μg/mL (R&D Systems), PC3B1a CM, or BC3B1a + J8H CM. After 72 hours, cells were washed with PBS and incubated 2 hours at 37°C with pretreatment solution to neutralize lysosomal β-galactosidase activity. The senescence-associated β-galactosidase (SA-β-gal) substrate solution was then added to the cells for an additional 4 hours. The cells were washed with PBS, harvested by trypsinization, and fluorescence intensity analyzed by flow cytometry.

Results

J8H antibody blocks ITGA6 cleavage and invasion without altering adhesion to laminin 511 *in vitro*

Monoclonal antibodies that bind the extracellular domain of integrins can either block normal adhesion and signaling functions or constitutively activate the integrin (28–30). Our previous work has established that a truncated form of ITGA6, called A6p, is produced by proteolytic cleavage of ITGA6 on the cell surface during cell migration on laminin coated surfaces (21, 22). A6p contains the transmembrane and cytoplasmic domains of ITGA6 and is required for cell migration and invasion, whereas A6N includes the ligand-binding region of the molecule (16). The PC3B1a cell line, which was previously established by *in vivo* selection for bone-homing capacity, displays constitutive production of A6p and A6N (Fig. 1A). Incubation of PC3B1a cells with the J8H antibody inhibits production of the cleaved products, whereas J1B5 and GoH3 antibodies have no effect on A6p production. The GoH3 and J1B5 antibodies are specific for ITGA6 and inhibit both the adhesion and migration function of ITGA6 (23, 24). Similarly, the AIIB2 antibody is a function blocking antibody specific for ITGB1 that prevents both adhesion and migration on laminin. Importantly, the J8H antibody inhibits cell migration but does not alter cell adhesion to laminin 511 (Fig. 1B and C).

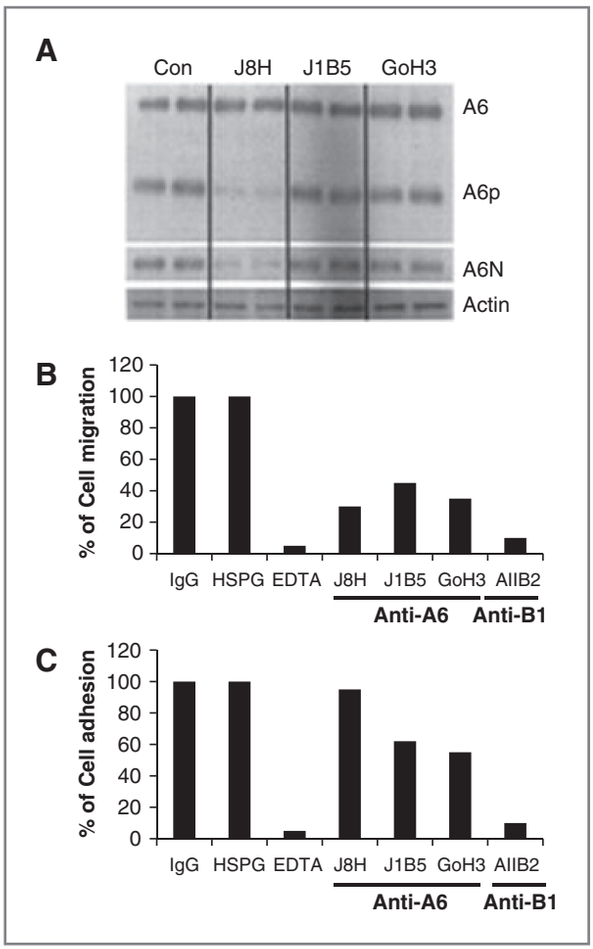

Figure 1. J8H antibody prevents ITGA6 cleavage and inhibits migration. A, PC3B1a cells were incubated with ITGA6 function-blocking antibodies for 48 hours and whole cell lysates assayed for the full length (A6), membrane-bound cleaved fraction (A6p), or amino terminal domain (A6N). Lanes represent duplicate-treated samples. B, cell migration through laminin-coated transwell inserts was assayed in the presence of the indicated neutralizing antibody specific for ITGA6 (J8H, J1B5, GoH3) or ITGB1 (AIIB2). Data are presented as % of control, which is isotype matched, nonspecific immunoglobulin (IgG). The non-antibody negative control is heparin sulfate proteoglycan (HSPG) and the non-antibody positive control is EDTA. C, PC3B1a cells were assayed for adhesion to a laminin 511–coated plate in the presence or absence of the indicated reagent. Data are presented as % control, where control is IgG as above.

Treatment with J8H antibody reduces lesion progression in a xenograft model

Our previous work demonstrated that inhibition of A6p production by J8H treatment delays, but does not prevent prostate tumor homing to bone (21). To investigate the efficacy of J8H as a noncytotoxic treatment of early disseminated cancer in bone, PC3B1a cells were injected into the arterial circulation of SCID mice. This cell line was selected for its bone-trophic

Published OnlineFirst April 16, 2014; DOI: 10.1158/1535-7163.MCT-13-0962

phenotype, reproducible aggressive metastasis formation, and constitutive expression of intact ITGA6 and ITGA6p. Animals were randomly assigned to control or treatment groups before tumor detection and intravenous administration of 4 mg/kg J8H antibody was initiated 1 week after cell injection as indicated in the study design (Fig. 2). Preliminary experiments demonstrated the presence of circulating antibody well beyond the 1 week treatment interval (data not shown). Osseous tumor growth was monitored by weekly micro-CT imaging and volumetric analysis. Lesions were recorded only when detected in all 3 views by micro-CT (axial, coronal, and sagittal).

Twenty-two of 24 mice developed bone lesions that were identified by micro-CT in the third week and 1 additional animal in the J8H treatment group developed a visible lesion at week 6. Initial tumor volumes were comparable in the J8H-treated and -untreated control groups at 3 weeks and the number of detectable lesions in each group at the outset was not significantly different ($n = 24$ and 26, respectively). Figure 2 shows a representative micro-CT image series of 2 animals with the region of interest (ROI) used for analysis. Evaluation of tumor volume in each lesion at termination demonstrated a trend of reduced tumor volume in the J8H treatment group; however, the intragroup variation negated statistical significance (untreated mean = 1.16 $\pm$ 0.96 mm^3; J8H-treated mean = 0.8 $\pm$ 1.02 mm^3; $P = 0.488$). At week 4, radiographic progression was apparent in nearly 40% of the lesions in untreated animals, whereas only 17% of the J8H-treated tumors showed an increase in lesion volume (Fig. 3A). By week 5, over 80% of the untreated lesions demonstrated progression compared with 45% in the J8H-treated group. Regression, defined as any decrease in tumor volume over time, was seen in 30% of lesions in the J8H-treated group, whereas only 11% of the untreated group demonstrated any degree of tumor reduction (data not shown). There was also a statistically significant difference in the specific growth rate between the treated and untreated groups over the entire time course of the study (Fig. 3B). The mean specific growth rate of the J8H-treated group was 0.109%/day [95% confidence interval (CI), 0.0767–0.142] compared with 0.187%/day (95% CI, 0.141–0.232) in the untreated animals ($P < 0.01$). Specific growth rate is calculated as "percent increase/day" (%/d) and is considered more accurate than doubling time for *in vivo* measure (31).

J8H-treated animals demonstrate a survival advantage

Although bone lesion progression was markedly reduced in J8H-treated animals, the question remained whether this would reflect a survival benefit. Animal protocols dictated the removal of any animals that appeared distressed or those for which the radiologist (without knowledge of the treatment groups) indicated fracture was imminent. Survival advantage was determined using log-rank analysis of the Kaplan–Meier survival time. Animals receiving the J8H antibody

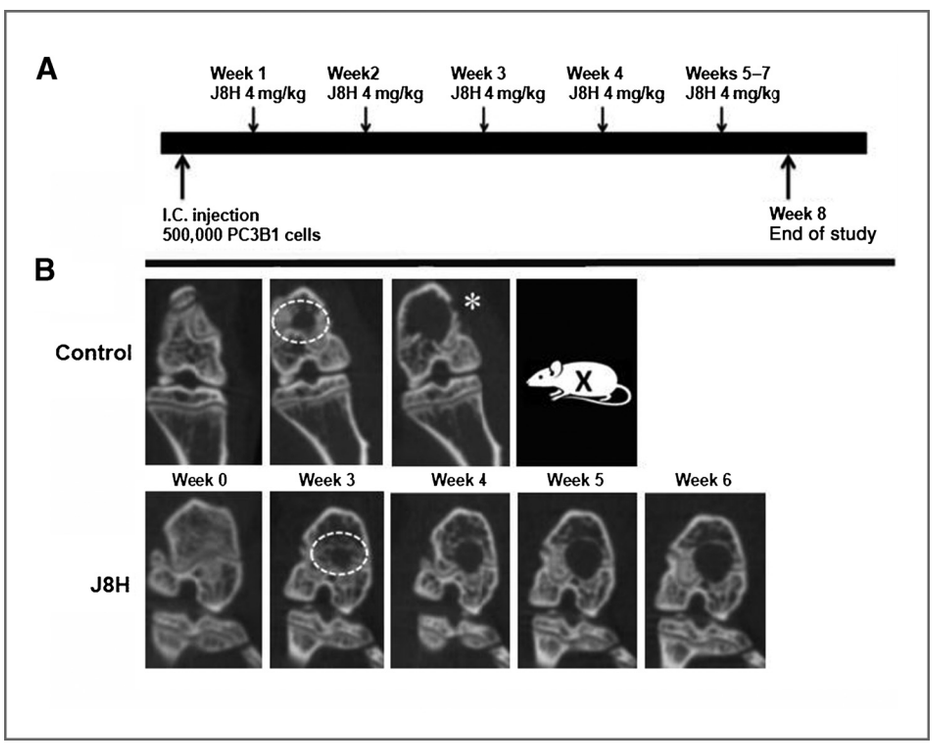

Figure 2. Study design.
A, schematic illustrating the animal protocol including intracardiac injection (I.C. injection) with prostate cancer cells (PC3B1a) and weekly tail vein injections of antibody (J8H, 4 mg/kg).
B, representative micro-CT scans of control vs. J8H-treated animals are shown before injection (Wk 0) or weekly beginning with week 3, which is the first point that radiographic lesions could be detected. The ROI used for lesion volume analysis is shown (white dotted circle). Animals were removed from the study (X) when imminent fracture was indicated by the radiologist (*).

Published OnlineFirst April 16, 2014; DOI: 10.1158/1535-7163.MCT-13-0962

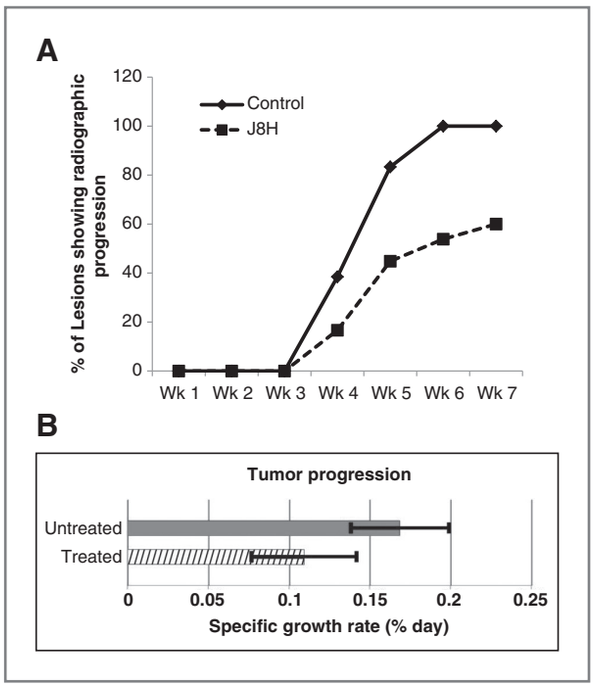

Figure 3. Quantitative analysis of tumor progression. A, metastatic bone lesions were recorded if detected in 3 views by micro-CT (axial, coronal, and sagittal) as lytic lesions. The osteolyic lesions ($n = 69$) were followed weekly by micro-CT analysis in untreated animals (solid line, diamonds, $n = 9$) or J8H-treated animals (dashed line, squares, $n = 13$). The untreated lesions ($n = 29$) and treated lesions ($n = 40$) were scored for progression by the radiologist without knowledge of the treatment groups. B, serial lesion volumes were used to determine the rate of tumor progression over time. Significance was determined using the Kruskal–Wallis nonparametric analysis ($P < 0.01$).

demonstrated a statistically significant survival advantage, with a median survival time of 41 days (SE = 3.5) compared with 34 days (SE = 2.2) in the control group ($P < 0.05$; Fig. 4). All animals in the untreated group were dead at 50 days, where as 30% of the J8H-treated mice survived and remained alive at the end of the study, for example, 8 weeks after systemic tumor injections.

Arrested tumor progression is associated with sclerotic bone reaction

Inspection of the images from animals with a J8H survival benefit revealed an unanticipated finding of lesions containing a sclerotic rim of reactive bone. Representative 3-dimensional micro-CT views of the lesions (Fig. 5A) indicated a well-circumscribed lesion observed within the axial, coronal, and sagittal views. Companion histology of the lesion demonstrated the presence of tumor in the trabecular bone (Fig. 5B), abutting the epiphyseal plate. The tumor was surrounded by fibroblasts and microvessels giving the appearance of granulation tissue as is seen in wound healing. Retrospective analysis of the lesions indicated that 67% of lesions ($n = 29$) in mice treated with the anti-ITGA6 antibody demonstrated features of a sclerotic bone reaction, compared with 33% of lesions ($n = 39$) in the untreated animals. Taken together, the data indicate that inhibition of ITGA6 cleavage *in vivo* reduces osteolytic tumor activity and induces a sclerotic reaction in bone lesions.

Engagement of ITGA6 with J8H induces tumor production of soluble factors

Secreted proteins that interact with the extracellular matrix have been shown to modify cellular response to the microenvironment via interaction with integrin receptors, including ITGA6. Specifically, the matricellular protein cysteine-rich protein 61 (CCN1/CYR61) has been implicated in both cutaneous wound healing and bone remodeling (32, 33). To determine if ITGA6 engagement affects tumor cell production of CCN1, conditioned media was collected from PC3B1a cells treated with J8H antibody for 24, 48, or 72 hours. ELISA assay for secreted CCN1 demonstrates a time-dependent increase in the production of CCN1 by cells with extracellular engagement of ITGA6 (Fig. 6). The PC2B1a and PC3B1a + J8H CM was tested for biologic function using an HFF senescence assay. In these experiments, HFFs are incubated with conditioned media from antibody-treated PC3B1a cells for 72 hours. HFF cells are then assayed for SA-β-Gal activity. Incubation of the HFF cells in serum-deprived media alone induces a low level of senescence, as indicated by SA-β-Gal activity (Fig. 6B). Treatment of the HFF cells with recombinant CCN1 (5 μg/mL) induces SA-β-Gal activity by 19% compared with control cells. Conditioned media collected from antibody treated PC3B1a cells resulted in a 61% increase in SA-β-Gal activity,

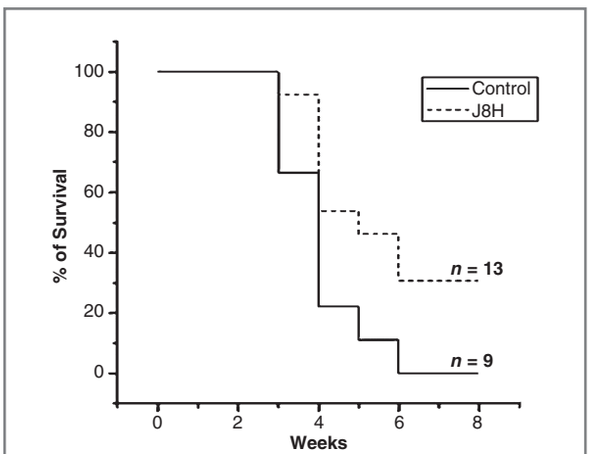

Median survival time

Group	n	Median survival (days)	SE	95% CI
Control	9	34	2.18	27–41
J8H	13	41	3.51	34–50

Figure 4. Survival advantage of J8H-treated animals. Survival advantage of the J8H-treated animals was determined using log rank analysis of the Kaplan–Meier survival time. Animals were followed for up to 8 weeks and were sacrificed if an imminent fracture in any lesion was detected by the radiologist, as dictated by the protocol.

Published OnlineFirst April 16, 2014; DOI: 10.1158/1535-7163.MCT-13-0962

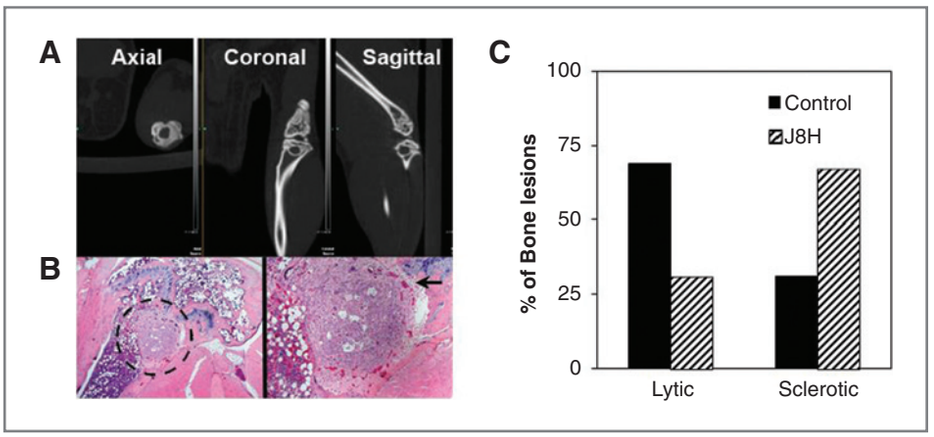

Figure 5. J8H-treated animals demonstrate a higher frequency of sclerotic lesions. A, axial, coronal, and sagittal views demonstrate reactive bone surrounding the osteolytic lesions. B, matched histologic sections obtained at the end of the study of the lesion in A. The black dotted circle defines PC3B1a prostate tumor growth abutting the epiphyseal plate. Increased magnification of the lesion demonstrates a sclerotic type lesion, encircled by vessels and new bone formation. C, the frequency of lytic or sclerotic lesions was scored by a radiologist using micro-CT images from untreated ($n = 29$) or J8H-treated ($n = 40$) animals. Individual lesions were evaluated at the end of the study, and data are presented as % of total lesions.

compared with 42% increase by conditioned media from cells without J8H treatment. These data indicate that both recombinant CCN1 alone and conditioned media (containing CCN1) collected from antibody treated PC3B1a cells, resulted in increased HFF senescence.

Discussion

Metastatic tumors in the bone marrow are typically refractory to standard chemotherapy and radiation treatment (5, 6). The mechanism(s) of resistance can be related to intrinsic characteristics of the tumor or mediated by the tumor microenvironment. Because of the significant contribution of the bone marrow microenvironment, many of the therapeutic strategies currently under development are designed to target not only the tumor itself, but the bone marrow microenvironment and the tumor/bone interface. For example, the bisphosphonate zoledronic acid is FDA approved for the treatment of prostate cancer–induced skeletal-related events (SRE). Another bone-targeted agent currently in clinical trials is denosumab, which is a monoclonal antibody that blocks osteoclast activation by inhibiting the receptor-activated NF-κβ ligand (RANKL; ref. 34). These agents have shown efficacy in reducing tumor progression, but are not without systemic effects on bone metabolism, and both have been implicated in osteonecrosis of the jaw (ONJ) disease and pathologic fractures.

Integrins are critical intermediaries in cell/microenvironment communication and thus represent a highly

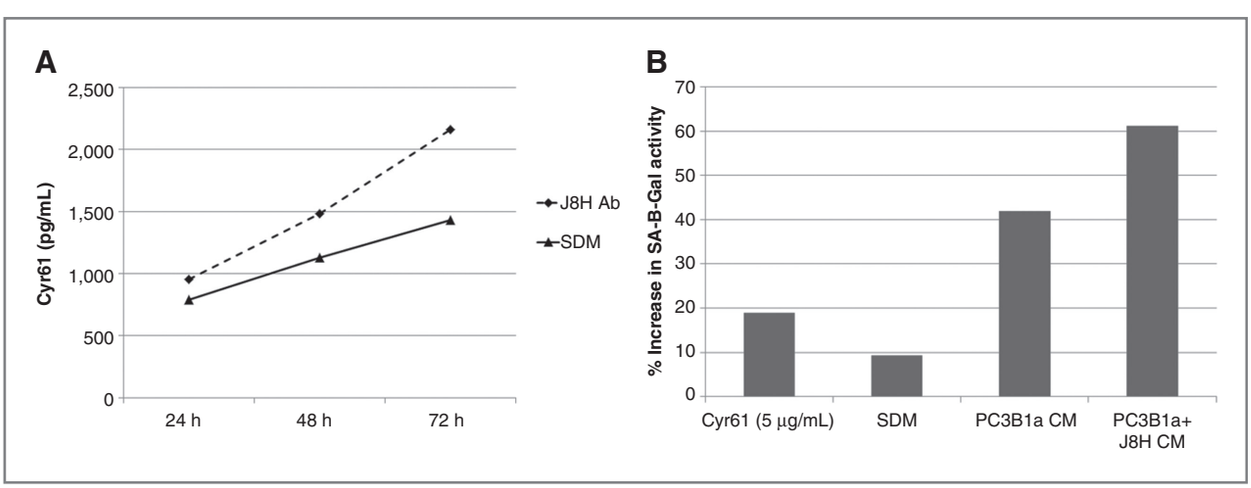

Figure 6. Soluble factors produced by PC3B1a cells with extracellular engagement of ITGA6. A, PC3B1a cells were incubated with J8H antibody for the indicated time, and the conditioned media collected and analyzed for Cyr61 concentration by ELISA assay. Concentration was calculated based on standard curve. B, PC3B1a CM or serum-deprived media (SDM) prepared in the presence or absence of J8H antibody engagement was incubated with HFF cells for 72 hours, followed by incubation with β-galactosidase substrate for 4 hours. Cells were then harvested and analyzed for SA-β-Gal activity by flow cytometry.

Published OnlineFirst April 16, 2014; DOI: 10.1158/1535-7163.MCT-13-0962

attractive target in oncology therapy (35, 36). Although many approaches to targeting integrin receptors have focused on the development of the tripeptide arginyl-glycyl-aspartic acid (RGD)-based therapeutics, most notably the pentapeptide Cilengitide (37), our work utilizes a function-blocking antibody specific for ITGA6, a laminin receptor that does not recognize RGD-containing ligands. ITGA6 has been identified as a stem cell marker and is expressed by more than 70% of advanced prostate carcinomas. Targeting laminin-binding integrins is particularly relevant to bone metastatic lesions as bone is a laminin-rich environment that provides a protective adhesion site for early metastatic tumors to survive standard chemotherapeutic agents (38–40). Importantly, the J8H antibody will block tumor migration without altering cell adhesion to laminin, as loss of ITGA6 adhesion by either circulating auto-antibody or ITGA6 mutation has been associated with epithelial blistering and basement membrane separation (41, 42). Control experiments demonstrated no direct effect of the antibody on cell proliferation or survival in short-term assays (data not shown). J8H recognizes both human and mouse integrin A6 and blocks A6p production but does not inhibit adhesion, which may be one reason for its low *in vivo* toxicity. J8H does inhibit tumor cell migration; however, it remains to be determined if normal cell migration, such as induced by wound healing, would be affected by J8H. In addition, we do not yet know the specific effects of J8H antibody treatment on hematopoietic stem cells and other normal cells in the bone marrow. However, we found no adverse effects or evidence of toxicity in the J8H-treated animals.

Bone-resident tumors induce a dysregulation of normal bone remodeling and can appear as either osteolytic or osteoblastic lesions (reviewed in refs. 43 and 44). Osteolytic lesions appear more frequently in patients with advanced breast cancer, whereas patients with metastatic bone lesions of prostate cancer are often osteoblastic, and the vast majority of patients display mixed osteolytic and osteoblastic bone disease. The molecular basis for the establishment of osteolytic versus osteoblastic bone metastasis in patients is not well understood and has been characterized as a vicious cycle driven by factors derived from both the tumor and the environment. In this study, inhibition of the cell-surface ITGA6 cleavage reaction, and not the adhesion function of the integrin, significantly decreased bone lesion progression. Sequential micro-CT imaging of animals in the J8H treatment group showed a frequent conversion of the scores from osteolytic to sclerotic lesions with a well-circumbscribed rim of increased density immediately surrounding the tumor. Interestingly, all lytic lesions progressed independent of treatment conditions until 4 weeks of treatment, when more than 60% of the lesions converted to sclerotic lesions over the remainder of the study. Taken together, these data suggest that the J8H treatment may affect the long-term host reaction to bone-resident tumor cells rather than blocking the early onset lytic process.

Although 100% of the surviving mice contained sclerotic lesions, it is an important limitation that only 4 mice survived to the end of the study. An increased number of mice would be needed to verify the dominance of the sclerotic lesions for predicting the increased survival of the mice, especially given the coexpression of lytic and blastic lesions. This study mimics the clinical situation in 2 important ways: the J8H antibody was delivered after lesions were detected in live animals by micro-CT and lesion progression; identification and scoring of sclerotic lesions in the same live animals was done by a board-certified radiologist. A future histomorphometric analysis using higher resolution images and isolated femurs at each time point could be done to provide additional details and insight about the changes in bone morphology.

Clinically, the development of sclerotic lesions is often considered curative (45, 46) and has been described as a "flare phenomenon" in which patients respond to bone metastasis treatment but have unexpected transient increases in alkaline phosphatase and show positive Technetium-99m-polyphosphate bone scans (47). Sclerotic lesions are considered benign-type lesions that progress slowly, involve a host reaction for entombment of the tumor, and are less painful than lytic-type lesions (48). Our data suggest that lesion conversion may be an indirect effect of ITGA6 engagement, perhaps by altering the secretome of the tumor in bone marrow. Fibroblast senescence is associated with cutaneous wound healing, and has been shown to be dependent on CCN1 binding to ITGA6 (49). *Ex vivo* analysis indicates that CCN1 seems to be a component of the soluble factors produced when cell motility is blocked; however, the functional effects on adjacent stromal components are likely to be multifactorial, and characterization of the mechanisms responsible for lesion conversion will require a more comprehensive approach (50). CCN1 likely is not the only factor in the conditioned media that causes senescence. Future studies using a broad-based proteomic approach may reveal additional senescence and growth regulatory factors.

The targeting of the extracellular domain of ITGA6, independent of the ligand-binding region may represent a new noncytotoxic approach for prostate patients with advanced disease and extensive skeletal involvement. Using a noncytotoxic approach to alter the cell–cell interactions and break the cycle of bone destruction may provide disease control without systemic toxicity.

Disclosure of Potential Conflicts of Interest

No potential conflicts of interest were disclosed.

Authors' Contributions

Conception and design: T.H. Landowski, A.E. Cress
Development of methodology: J. Gard, R.B. Nagle

Published OnlineFirst April 16, 2014; DOI: 10.1158/1535-7163.MCT-13-0962

Acquisition of data (provided animals, acquired and managed patients, provided facilities, etc.): J. Gard, E. Pond, G.D. Pond, R.B. Nagle
Analysis and interpretation of data (e.g., statistical analysis, biostatistics, computational analysis): T.H. Landowski, J. Gard, E. Pond, G.D. Pond, C.P. Geffre, A.E. Cress
Writing, review, and/or revision of the manuscript: T.H. Landowski, J. Gard, E. Pond, G.D. Pond, R.B. Nagle, C.P. Geffre, A.E. Cress
Administrative, technical, or material support (i.e., reporting or organizing data, constructing databases): J. Gard
Study supervision: A.E. Cress

Acknowledgments

Immunohistochemical support was provided by the Tissue Acquisition and Cellular/Molecular Analysis Shared Service (TACMASS) and xenograft services were provided by the Experimental Animal Shared Service (EMSS) supported by the University of Arizona Cancer Center. The authors especially thank B. Skovan and W. Meek for the excellent technical support (animal injections and bone histopathology, respectively) and W.L. Harryman for editorial assistance.

Grant Support

This work was supported by RO1 CA159406 and P30 CA023074 (A.E. Cress) and P01 CA017094 (T.H. Landowski and R.B. Nagle).

The costs of publication of this article were defrayed in part by the payment of page charges. This article must therefore be hereby marked *advertisement* in accordance with 18 U.S.C. Section 1734 solely to indicate this fact.

Received November 15, 2013; revised March 6, 2014; accepted April 2, 2014; published OnlineFirst April 16, 2014.

References

1. Zheng Y, Zhou H, Dunstan CR, Sutherland RL, Seibel MJ. The role of the bone microenvironment in skeletal metastasis. J Bone Oncol 2013;2:47–57.
2. Thobe M, Clark RJ, Bainer RO, Prasad SM, Rinker-Schaeffer CW. From prostate to bone: key players in prostate cancer bone metastasis. Cancers 2011;3:478–93.
3. Liu W, Laitinen S, Khan S, Vihinen M, Kowalski J, Yu G, et al. Copy number analysis indicates monoclonal origin of lethal metastatic prostate cancer. Nat Med 2009;15:559–65.
4. Robbins CM, Tembe WA, Baker A, Sinari S, Moses TY, Beckstrom-Sternberg S, et al. Copy number and targeted mutational analysis reveals novel somatic events in metastatic prostate tumors. Genome Res 2011;21:47–55.
5. Morris MJ, Scher HI. Clinical approaches to osseous metastases in prostate cancer. Oncologist 2003;8:161–73.
6. Sturge J, Caley MP, Waxman J. Bone metastasis in prostate cancer: emerging therapeutic strategies. Nat Rev Clin Oncol 2011;8:357–68.
7. Cress AE, Rabinovitz I, Zhu W, Nagle RB. The α6 β1 and α6 β4 integrins in human prostate cancer progression. Cancer Metastasis Rev 1995;14:219–28.
8. Friedrichs K, Ruiz P, Franke F, Gille I, Terpe HJ, Imhof BA. High expression level of α6 integrin in human breast carcinoma is correlated with reduced survival. Cancer Res 1995;55:901–6.
9. Yamamoto H, Masters JR, Dasgupta P, Chandra A, Popert R, Freeman A, et al. CD49f is an efficient marker of monolayer- and spheroid colony-forming cells of the benign and malignant human prostate. PLoS ONE e46979 doi. 2012;7:11.
10. Lathia JD, Gallagher J, Heddleston JM, Wang J, Eyler CE, MacSwords J, et al. Integrin α6 regulates glioblastoma stem cells. Cell Stem Cell 2010;6:421–32.
11. Gu YC, Kortesmaa J, Tryggvason K, Persson J, Ekblom P, Jacobsen SE, et al. Laminin isoform-specific promotion of adhesion and migration of human bone marrow progenitor cells. Blood 2003;101:877–85.
12. Notta F, Doulatov S, Laurenti E, Poeppl A, Jurisica I, Dick JE. Isolation of single human hematopoietic stem cells capable of long-term multilineage engraftment. Science 2011;333:218–21.
13. Qian H, Georges-Labouesse E, Nystrom A, Domogatskaya A, Tryggvason K, Jacobsen SE, et al. Distinct roles of integrins α6 and α4 in homing of fetal liver hematopoietic stem and progenitor cells. Blood 2007;110:2399–407.
14. Domogatskaya A, Rodin S, Boutaud A, Tryggvason K. Laminin-511 but not -332, -111, or -411 enables mouse embryonic stem cell self-renewal *in vitro*. Stem Cells 2008;26:2800–9.
15. Siler U, Seiffert M, Puch S, Richards A, Torok-Storb B, Müller CA, et al. Characterization and functional analysis of laminin isoforms in human bone marrow. Blood 2000;96:4194–203.
16. Demetriou MC, Cress AE. Integrin clipping: a novel adhesion switch? J Cell Biochem 2004;91:26–35.
17. Demetriou MC, Pennington ME, Nagle RB, Cress AE. Extracellular α6 integrin cleavage by urokinase-type plasminogen activator in human prostate cancer. Exp Cell Res 2004;294:550–8.
18. Sheng S. The urokinase-type plasminogen activator system in prostate cancer metastasis. Cancer Metastasis Rev 2001;20:287–96.
19. Shariat SF, Roehrborn CG, McConnell JD, Park S, Alam N, Wheeler TM, et al. Association of the circulating levels of the urokinase system of plasminogen activation with the presence of prostate cancer and invasion, progression, and metastasis. J Clin Oncol 2007;25:349–55.
20. Pawar SC, Demetriou MC, Nagle RB, Bowden GT, Cress AE. Integrin α6 cleavage: a novel modification to modulate cell migration. Exp Cell Res 2007;313:1080–9.
21. Ports MO, Nagle RB, Pond GD, Cress AE. Extracellular engagement of α6 integrin inhibited urokinase-type plasminogen activator-mediated cleavage and delayed human prostate bone metastasis. Cancer Res 2009;69:5007–14.
22. Sroka IC, Pond GD, Nagle RB, Porreca F, King T, Pestano G, et al. Human cell surface receptors as molecular imaging candidates for metastatic prostate cancer. Open Prost Cancer J 2009;2:59–66.
23. Hogervorst F, Kuikman I, Noteboom E, Sonnenberg A. The role of phosphorylation in activation of the α6A β1 laminin receptor. J Biol Chem 1993;268:18427–30.
24. Damsky CH, Librach C, Lim KH, Fitzgerald ML, McMaster MT, Janatpour M, et al. Integrin switching regulates normal trophoblast invasion. Development 1994;120:3657–66.
25. Sonnenberg A, Janssen H, Hogervorst F, Calafat J, Hilgers J. A complex of platelet glycoproteins Ic and IIa identified by a rat monoclonal antibody. J Biol Chem 1987;262:10376–83.
26. Sroka IC, Chen ML, Cress AE. Simplified purification procedure of laminin-332 and laminin-511 from human cell lines. Biochem Biophys Res Commun 2008;375:410–3.
27. King TE, Pawar SC, Majuta L, Sroka IC, Wynn D, Demetriou MC, et al. The role of α6 integrin in prostate cancer migration and bone pain in a novel xenograft model. PLoS ONE 2008;3:e3535.
28. Ginsberg MH, Partridge A, Shattil SJ. Integrin regulation. Curr Opin Cell Biol 2005;17:509–16.
29. Hynes RO. Integrins: bidirectional, allosteric signaling machines. Cell 2002;110:673–87.
30. Tsuchida J, Ueki S, Saito Y, Takagi J. Classification of 'activation' antibodies against integrin β1 chain. FEBS Lett 1997;416:212–6.
31. Mehrara E, Forssell-Aronsson E, Ahlman H, Bernhardt P. Specific growth rate versus doubling time for quantitative characterization of tumor growth rate. Cancer Res 2007;67:3970–5.
32. Si W, Kang Q, Luu HH, Park JK, Luo Q, Song W-X, et al. CCN1/Cyr61 is regulated by the canonical Wnt signal and plays an important role in Wnt3A-induced osteoblast differentiation of mesenchymal stem cells. Mol Cell Biol 2006;26:2955–64.
33. Leask A, Abraham DJ. All in the CCN family: essential matricellular signaling modulators emerge from the bunker. J Cell Sci 2006;119:4803–10.
34. Saylor PJ, Armstrong AJ, Fizazi K, Freedland S, Saad F, Smith MR, et al. New and emerging therapies for bone metastases in genitourinary cancers. Eur Urol 2013;63:309–20.
35. Desgrosellier JS, Cheresh DA. Integrins in cancer: biological implications and therapeutic opportunities. Nat Rev Cancer 2010;10:9–22.

Published OnlineFirst April 16, 2014; DOI: 10.1158/1535-7163.MCT-13-0962

36. Weis SM, Cheresh DA. αV integrins in angiogenesis and cancer. Cold Spring Harb Perspect Med 2011;1:a006478.
37. Reardon DA, Cheresh D. Cilengitide: a prototypic integrin inhibitor for the treatment of glioblastoma and other malignancies. Genes Cancer 2011;2:1159–65.
38. David E, Blanchard F, Heymann MF, De PG, Gouin F, Redini F, et al. The bone niche of chondrosarcoma: a sanctuary for drug resistance, tumour growth and also a source of new therapeutic targets. Sarcoma 2011;2011:932451.
39. Hazlehurst LA, Landowski TH, Dalton WS. Role of the tumor microenvironment in mediating *de novo* resistance to drugs and physiological mediators of cell death. Oncogene 2003;22: 7396–402.
40. Semenas J, Allegrucci C, Boorjian SA, Mongan NP, Persson JL. Overcoming drug resistance and treating advanced prostate cancer. Curr Drug Target 2012;13:1308–23.
41. Rashid KA, Stern JN, Ahmed AR. Identification of an epitope within human integrin α6 subunit for the binding of autoantibody and its role in basement membrane separation in oral pemphigoid. J Immunol 2006;176:1968–77.
42. Mignogna M, Lanza A, Rossiello L, Ruocco V, Ahmed AR. Comparison of reactivity and epitope recognition between sera from American and Italian patients with oral pemphigoid. Clin Exp Immunol 2006;145: 28–35.
43. Roodman GD. Mechanisms of bone metastasis. Discov Med 2004;4:144–8.
44. Sterling JA, Edwards JR, Martin TJ, Mundy GR. Advances in the biology of bone metastasis: how the skeleton affects tumor behavior. Bone 2011;48:6–15.
45. Scher HI, Morris MJ, Basch E, Heller G. End points and outcomes in castration-resistant prostate cancer: from clinical trials to clinical practice. J Clin Oncol 2011;29:3695–704.
46. Yamashita Y, Aoki T, Hanagiri T, Yoshii C, Mukae H, Uramoto H, et al. Osteosclerotic lesions in patients treated with gefitinib for lung adenocarcinomas: a sign of favorable therapeutic response. Skeletal Radiol 2012;41:409–14.
47. Hashisako M, Wakamatsu K, Ikegame S, Kumazoe H, Nagata N, Kajiki A. Flare phenomenon following gefitinib treatment of lung adenocarcinoma with bone metastasis. Tohoku J Exp Med 2012;228:163–8.
48. Conti G, La Torre G, Cicalese V, Micheletti G, Ludovico MG, Vestita GD, et al. Prostate cancer metastases to bone: observational study for the evaluation of clinical presentation, course and treatment patterns. Presentation of the METAURO protocol and of patient baseline features. Arch Ital Urol Androl 2008;80:59–64.
49. Jun JI, Lau LF. The matricellular protein CCN1 induces fibroblast senescence and restricts fibrosis in cutaneous wound healing. Nat Cell Biol 2010;12:676–85.
50. Chiechi A, Novello C, Magagnoli G, Petricoin EF, Deng J, Benassi MS, et al. Elevated TNFR1 and serotonin in bone metastasis are correlated with poor survival following bone metastasis diagnosis for both carcinoma and sarcoma primary tumors. Clin Cancer Res 2013;19: 2473–85.

Published OnlineFirst April 16, 2014; DOI: 10.1158/1535-7163.MCT-13-0962

Molecular Cancer Therapeutics

Targeting Integrin α6 Stimulates Curative-Type Bone Metastasis Lesions in a Xenograft Model

Terry H. Landowski, Jaime Gard, Erika Pond, et al.

Mol Cancer Ther 2014;13:1558-1566. Published OnlineFirst April 16, 2014.